Chemical Research in Toxicology

pubs.acs.org/crt

Article

Isolation, Characterization, and Toxicity Study of Stress Degradation Products of Pranlukast Hydrate

Krunal J. Prajapati and Charmy S. Kothari*

Cite This: *Chem. Res. Toxicol.* 2022, 35, 1206−1219

Read Online

ACCESS | Metrics & More | Article Recommendations | Supporting Information

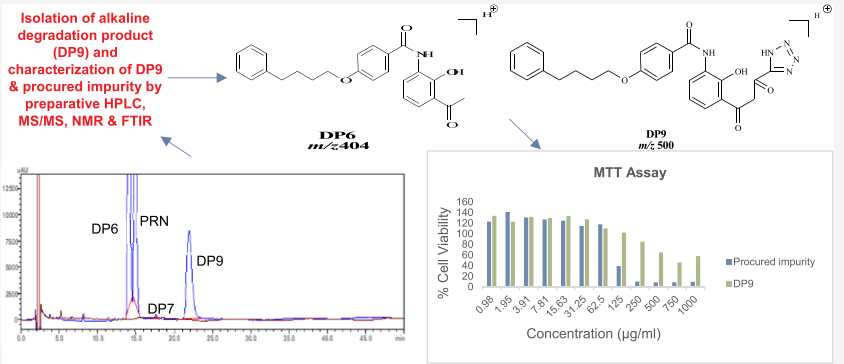

ABSTRACT: Pranlukast hydrate (PRN), a cysteinyl leukotriene receptor antagonist ($CysLT_1$), is used to treat bronchial asthma. The objective of this study is to perform the isolation, characterization, and toxicity analysis of stress degradation products of PRN. In high-performance liquid chromatography (HPLC), the separation was achieved using a Phenomenex Gemini C18 (250 × 4.6 mm, 5 μ) column; the ammonium format buffer (50 mM), pH 4, with formic acid: acetonitrile (50:50, v/v) was used as a mobile phase at a flow rate of 1.25 mL/min; and the photodiode array detector was used for detection at 230 nm. The drug was subjected to stress degradation as per ICH Q1A (R2) and ICH Q1B guidelines. The drug was found to be labile in alkaline (62.48% degradation) and photolytic (liquid state) (7.67% degradation) conditions, whereas the drug was found to be stable in acidic, peroxide, photolytic (solid state), and thermal conditions. The characterization of the drug and its degradation products was achieved using liquid chromatography−electrospray ionization−quadrupole time of flight tandem mass spectrometry (LC-ESI-QTOF-MS/MS), and the degradation mechanism was proposed. There were two degradation products observed in alkaline conditions (DP6 and DP9), whereas six novel degradation products were observed in photolytic degradation products (DP1, DP3, DP4, DP5, DP7, and DP10). The developed method was successfully validated as per the ICH Q2 (R1) guideline. The isolation of the alkaline degradation product DP9 was performed using preparative HPLC, and it was found to be 96.8% pure degradation product. The characterizations of the isolated degradation product (DP9) and procured impurity were performed using MS/MS, NMR, and FTIR. The mass of the procured impurity and DP9 were observed to be 404 and 500 Da, respectively. The in vitro cytotoxicity study of the procured impurity and DP9 was conducted using a 3-(4,5 dimethylthiazol-2-yl)-2,5-diphenyl tetrazolium bromide (MTT) assay using an A549 cell line, and they were found to be cytotoxic at concentrations above 62.5 and 250 μg/mL, respectively. Furthermore, an in silico toxicity study was performed to predict the toxicity of all the major characterized degradation products of PRN using admetSAR software version 2.0. DP1, DP2, DP6, and DP10 were found to be hepatotoxic, mutagenic according to the micronucleus test, and aquatic toxic. We can conclude that the drug should be kept away from the direct exposure of light and the toxicity levels of DP1, DP2, DP6, and DP10 should be reduced below 0.1% to avoid their toxic effect.

INTRODUCTION

Pranlukast hydrate (PRN) {4-oxo-8-[4-(4-phenylbutoxy)-benzoylamino]-2-(tetrazole-5-yl)-4*H*-1-benzopyran hemihydrate}[1] is the first orally active, novel, potent, and selective cysteinyl leukotriene receptor antagonist ($CysLT_1$).[2,3] It is used in the treatment of asthma where it reduces the bronchospasm caused by the development of allergen-induced mega choline airway hyperresponsiveness and hence results in an excellent recovery of normal lung function within a short time.[2−4]

According to ICH Q1A (R2) and ICH Q1B guidelines, stress testing is the process of identifying degradation products (DPs)

Received: June 18, 2021
Published: June 22, 2022

generated by applying different stress conditions such as hydrolysis, oxidation, thermal, and photolysis. Furthermore, it helps establish the degradation pathway and the mechanism of formation of a DP. It also helps elucidate the intrinsic stability of the molecule.[5,6] The knowledge of the drug's DPs can help decrease the toxicity and side effects of the drug. Hence, the complete characterization of DPs is mandatory.[7] It provides information on how physical and chemical changes in a drug molecule can affect its quality, safety, and efficacy.

This drug is official in Japanese pharmacopeia (JP'17).[8] One stability-indicating reverse-phase high-performance liquid chromatography (RP-HPLC) method has reported.[9] Few RP-HPLC methods have reported of PRN in formulation,[10] PRN and its metabolism in plasma,[5,11] PRN pharmacokinetics in plasma,[12] and few LC−MS/MS (liquid chromatography−tandem mass spectrometry) methods have reported for PRN in plasma.[1,2,13] But no studies are available for the isolation and characterization of the stress DPs of this drug. Hence, the study aims to develop and validate a novel stability-indicating liquid chromatography−electrospray ionization−quadrupole time of flight tandem mass spectrometry (LC-ESI-QTOF-MS/MS) method for the determination of PRN along with isolation, in vitro and in silico toxicity study of major DPs of PRN. Based on the aim, the following are the objectives of this study: (1) to develop a novel mass compatible, simple, specific, selective, sensitive, linear, accurate, robust, precise, and stability-indicating method; (2) to perform a stress degradation study by LC−MS according to ICH Q1A (R2)[14] and ICH Q1B guidelines;[15] (3) to perform characterization of the drug and its DPs by LC-ESI-QTOF-MS/MS; (4) to perform validation as per ICH Q2 (R1)[16] guidelines; (5) isolation of major DPs by preparative HPLC and characterization of major DPs by MS/MS, nuclear magnetic resonance (NMR), and Fourier transform infrared (FTIR) spectroscopy; and (6) to perform an in vitro toxicity study using a 3-(4,5 dimethylthiazol-2-yl)-2,5-diphenyl tetrazolium bromide (MTT) assay and an in silico toxicity study using admetSAR software version 2.0[17] of major DPs.

EXPERIMENTAL SECTION

Materials and Reagents. The PRN active pharmaceutical ingredient (API) and sachets (10% w/w) were obtained as a complimentary sample from Cadila Pharmaceuticals Ltd. (Ahmedabad, India). HPLC-grade acetonitrile (ACN) was procured from Spectrochem (Mumbai, India). HPLC-grade formic acid was procured from Rankem (Bangalore, India). High-purity water was obtained from a Millipore Milli-Q water purification system (Millipore, Milford, MA, USA). Other analytical grade (AR) reagents—concentrated hydrochloric acid (HCl), sodium hydroxide (NaOH), hydrogen peroxide (30% H_2O_2), and ammonium format buffer—were procured from SD Fine Chemicals Limited (Mumbai, India).

Instrumentation. An auto-sampler HPLC Shimadzu SIL-20AC system (Shimadzu, Japan) is composed of a column oven (CTO-20AC), a quaternary pump (LC-20ADvp) with a degasser (DGU-20A5R), a system controller (CBM-20A SPD-M20A), and a photodiode array (PDA) detector. The Shimadzu LC 8030 instrument is attached to a TOF mass spectrometer with an ESI source in the positive and negative mode. Data analysis was carried out using Lab Solution software. The Bruker NMR instrument (Bruker, Switzerland) was used for recording ^1H and ^{13}C NMR spectra at frequencies of 400.13 and 100.61 MHz, respectively. Data analysis was carried out using Topspin software. The Jasco FTIR 6100 series (Jasco, Japan) was used to record the FTIR spectrum. Data analysis was carried out using Spectra Manager software. A Waters (Milford, MA, USA) preparative HPLC system equipped with a 515 HPLC pump and a 2489 UV−visible detector was used. Data analysis was carried out using Empower 2 software. The photostability chamber (Thermo Fischer, Mumbai, India), the vacuum oven (Samiksha Industrial Corporation, Mumbai, India), the pH meter (pH tutor, Eutech Instruments, USA), the digital analytical balance (CX-220, Citizen, USA), and the ultra-sonicator (D-compact, EIE Instruments Pvt Ltd., Ahmedabad, India) were used in this study.

Chromatographic and Mass Spectrometric Conditions. The chromatographic separation was achieved using a Phenomenex Gemini C18 column (250 × 4.6 mm, 5 μ) with a mobile phase consisted of ammonium format (50 mM), pH 4, with formic acid/ACN (50:50, v/v) in the isocratic mode at a flow rate of 1.25 mL/min. The chromatograms were monitored at 230 nm wavelength (λ). The column and auto-sampler temperatures were controlled to be 40 and 15 °C, respectively. The diluent used was water/ACN (50:50, v/v). The run time was 35 min. The ESI-QTOF-MS/MS operating conditions were as follows: ESI in the positive and negative ion mode was used for good mass signal sensitivity. Nitrogen was used as a drying gas (450 °C, 15 L/min) and a nebulizing gas (3 L/min). The desolvation temperature (DL) was 250 °C.

Preparation of the Stock Solution and Working Standard Solution. PRN is insoluble in water and methanol but soluble in dimethyl sulfoxide (DMSO) (10 mg/mL) and dimethylformamide (DMF) (20 mg/mL). Hence, the stock solution of PRN with a concentration of 1000 μg/mL was prepared by accurately weighing 10 mg of API in a 10 mL amber-color volumetric flask and dissolved with 3 mL of DMSO. The volume of the resulting solution was made up to the mark with ACN. From the stock solution, the working standard solution of PRN with a concentration of 100 μg/mL was prepared by taking a 1 mL aliquot in a 10 mL amber-color volumetric flask and made up the volume to the mark with a diluent.

Preparation of the Sample Solution. A PRN sample solution with a concentration of 1000 μg/mL was prepared by taking 10 sachets (equivalent to 1 g) into a mortar pestle and crushing. Then, powder equivalent to 100 mg was taken in a 100 mL amber-color volumetric flask. Further, 30 mL of DMSO was added, dissolved, and sonicated for 15 min. Then, the volume was made up to the mark with ACN. From the stock solution, a 100 μg/mL solution was prepared by taking a 1 mL aliquot in a 10 mL amber-color volumetric flask and made up the volume to the mark with a diluent.

Stress Degradation Studies. Stress degradation studies of PRN were performed under different stress conditions—hydrolysis (acidic, alkaline), oxidation, photolytic, and thermal, which were included in the specificity of the drug. The mass balance was calculated considering % assay + % degradation products + % impurities.[18]

Preparation of Stress Degradation Samples for Analysis. Hydrolytic degradation was performed by an acid (0.01 N ACN HCl) and an alkaline (0.1 N NaOH) for 7 days and 4 h, respectively, at 25 °C. Oxidative degradation was carried out using 3% ACN H_2O_2 at 25 °C. The ACN was used as a co-solvent because the drug was completely insoluble in water[19−22] and precipitated out in HCl and H_2O_2; however, it was slightly soluble at an alkaline pH, so alkaline degradation was performed without the addition of the co-solvent. Photolytic degradation was conducted using a diluent [DMSO/ACN (3:7, v/v)] in a liquid state, and the sample was kept in a photostability chamber (40 °C, 75% RH) for 1.2 million lux h, 200 W/m^2. While in the solid-state condition, the drug was spread on a Petri dush, covered with a transparent glass, and kept in a photostability chamber (40 °C, 75% RH) for 6 million lux h, 1000 W/m^2. Thermal degradation was performed by spreading the drug in an amber-color Petri dish, covered with a glass, and kept in a hot air oven at 100 °C for 7 days.

Acidic and alkaline stressors were neutralized by adding dropwise 0.01 N NaOH and 0.1 N HCl, respectively, till the pH became 7, which was confirmed using a pH strip.[23,24] The final concentration of 100 μg/mL was prepared by further diluting all the stressors with a blank. All the solutions were filtered using a 0.22 μ membrane syringe filter before analysis.

Method Validation. The developed method was validated by evaluating various parameters such as system suitability, linearity, limit of detection (LOD) and limit of quantification (LOQ), precision, accuracy, robustness, specificity, and selectivity as per ICH Q2 (R1)

https://doi.org/10.1021/acs.chemrestox.1c00222
Chem. Res. Toxicol. 2022, 35, 1206−1219

guidelines. The stock solution of 1000 μg/mL concentration was prepared and used in the measurement of all the parameters mentioned below.

The system suitability was characterized by injecting six replicates (n = 6) of 100 μg/mL concentration and evaluating the retention time (t_R), number of theoretical plates (NTP), tailing factor, area, and % relative standard deviation (% RSD). The linearity was characterized for concentration values of 50, 75, 100, 125, and 150 μg/mL (n = 2). The peak area (μAU) versus concentration (μg/mL) curves were plotted by using the linear regression method, and the slope, intercept, and correlation coefficient (r) were determined. The LOD and LOQ were calculated based on the standard deviation of the response and the slope. The precision study was conducted using three different concentrations, 50, 100, and 150 μg/mL (n = 3), on the same day and three consecutive days for the intra-day and inter-day precision, respectively; and the % RSD was calculated. The recovery study was performed using the standard addition method by spiking the standard into the sample using three different concentrations, 80, 100, and 120 μg/mL (n = 3), at three different levels, 80, 100, and 120%. The robustness was characterized by deliberate changes in all selected parameters as follows: mobile phase composition (±2), pH (±0.2), flow rate (±0.1 mL/min), and temperature (±5 °C) at a concentration of 100 μg/mL, and the % RSD was calculated. The specificity of the method was determined by checking the interference between the drug peak and the placebo, formulation, and DP peaks and studying the stress degradation behavior of PRN. Furthermore, the peak purity of the drug and the DP peaks were analyzed.

In Silico Toxicity Study. The physicochemical, absorption, distribution, metabolism, excretion, and toxicity (ADMET) properties of the PRN and its DPs were predicted using admetSAR software version 2.0 and QSAR toobox software. The physicochemical and ADME parameters were selected, including solubility, plasma protein binding, lipophilicity, human intestinal absorption, permeability, human oral bioavailability, transporters, cytochrome P450 (CYP) substrates, CYP inhibition, and receptor binding. The toxicity parameters were selected, including sensitization, Ames and micronuclear mutagenicity, carcinogenicity, hepatotoxicity, acute oral toxicity, and aquatic toxicity.

In Vitro Cytotoxicity Study.[25,26] The in vitro cytotoxicity study of DPs of PRN (procured impurity and DP9) was performed on an A549 cell line[27−32] using MTT[29] assays. Cells were observed using an inverted microscope to assess the degree of confluency and to confirm the absence of bacterial and fungal contamination. The cell layer was washed with 5 mL of sterile phosphate-buffered saline (PBS). PBS was removed, and cells were trypsinized with 1 mL of 0.25% trypsin for 2−5 min. After trypsinization, a 5 mL growth medium with 10% fetal bovine serum (FBS) was added to the flask. Cells were dislodged by taping the flask. Cells were pelleted out by centrifuging the cell culture at 800 rpm for 5 min. The cell pellet was resuspended in a growth medium and mixed to obtain a homogeneous cell suspension. Cells were counted using a hemocytometer and adjusted to contain a 1×10^5/mL concentration (1×10^4/well). Cell suspension (0.1 mL) was dispensed to each well of 96-well plates and incubated at 37 ± 1 °C in 5 ± 1% CO_2 in a humidified incubator for 24 h. At the end of the incubation period, different concentrations of the test item were added, and the plate was incubated at 37 °C for 24 ± 2 h. The procured impurity, DP9 (0.98, 1.95, 3.91, 7.81, 15.63, 31.25, 62.50, 125, 250, 500, 750, and 1000 μg/mL), positive control—sodium lauryl sulfate (SLS), and negative control (NC)—Dulbecco's modified Eagle's medium (DMEM) were tested in triplicate. At the end of incubation, media with test items were removed and replaced with DMEM containing 10% FBS. The MTT reagent [0.01 mL (5 mg/mL)] was added to each well. The plate was incubated at 37 ± 1 °C in 5 ± 1% CO_2 in a humidified incubator for 2 h. At the end of incubation, absorbance was determined in an enzyme-linked immune sorbent assay (ELISA) plate reader at 570 nm with 650 nm as a reference wavelength. The data are expressed as percentage cell viability versus concentration by taking the NC cell as 100% viable as given in the below equation.

$$\% \text{ viability} = \frac{\text{mean concentration of procured impurity/DP9}}{\text{mean concentration of NC}} \times 100$$

RESULTS AND DISCUSSION

Optimization of the Method. It was mandatory to optimize the chromatographic conditions to obtain a better resolution between the drug and its DPs. Based on the literature, where the trials were performed in different columns, it was proposed that the Phenomenex Gemini C_{18} column was more suitable for method development. Mobile phase trials were initiated with methanol and water with 0.01% ammonia[13] at different pH values and different ratios, but the peak shape was not good (NTP < 2000) and tailing (>2) was observed. Hence, to further improve the peak shape, the trials were taken with ammonium acetate and format buffer (different strength) with ACN or methanol in different ratios.[1,12] The peak shape was improved, but tailing was observed. Hence, different pH values were obtained with acetic acid or formic acid,[33] and finally, ammonium format buffer (pH 4 adjusted with formic acid)/ACN was used in an isocratic mode, which showed a symmetric peak (NTP > 2000, tailing < 2). To achieve the resolution between the drug and its DP peaks, the flow rate was optimized to be 1.25 mL/min. The wavelength was selected based on the mass balance approach at 230 nm. The column temperature was set at 40 °C for the improvement of the peak shape.

Finally, the resolution between the drug and its DPs was achieved by selecting a Phenomenex Gemini C18 (250 × 4.6 mm, 5 μ) column. The mobile phase was selected ammonium formate (50 mM), pH 4, with formic acid: ACN (50:50, v/v) at a flow rate of 1.25 mL/min. The wavelength was selected to be 230 nm, and the column temperature was set to be 40 °C (Figure S1).

Forced Degradation Studies.[34,35] The forced degradation study's objective was to separate the drug peak and all the degradation peaks effectively. Hence, no co-elution or interference of the unknown degradation peak was observed.

Degradation Behavior of PRN. The forced degradation study was carried out by using milder conditions initially. In hydrolysis (acidic and alkaline), degradation was initiated with 0.01 N ACN HCl and NaOH at 25 °C for 1 h. Still, no degradation was observed; hence, the concentration (0.1 N) and time interval were increased in an alkaline condition up to 4 h, which resulted in significant degradation (DP6, DP7, and DP9). In acidic hydrolysis, the higher concentration (0.1 N or above) was not taken because the sample was insoluble and precipitated out at lower pH,[2] so a low concentration (0.01 N) was taken for up to 7 days. In a peroxide condition, degradation was initiated with 3% ACN H_2O_2[26] at 25 °C for 1 h, but no degradation was observed, so the time was increased up to 24 h, but no significant degradation was observed (DP8). In a thermal condition, based on "a stress testing benchmarking study" and the melting point (233−235 °C) of PRN, degradation was initiated with a high temperature (100 °C) using a hot air oven, but no degradation was observed for up to 7 days. In a photolytic condition, the liquid sample was kept under a photostability chamber (40 °C, 75% RH) for 1.2 million lux h, 200 W/m^2, and significant degradation was observed (DP1, DP2, DP3, DP4, DP5, DP7, and DP10). In solid condition, the sample was kept under a photostability chamber (40 °C, 75% RH) for 1.2 million lux h, 200 W/m^2, but no degradation was observed, and upon

https://doi.org/10.1021/acs.chemrestox.1c00222
Chem. Res. Toxicol. 2022, 35, 1206−1219

Table 1. Summary of the Degradation Behavior of PRN and Its DPs[a]

Conditions	% Degradation	Resolution	RRT (min)	% Assay	Mass balance	Peak purity index
(1) Acidic hydrolysis (0.01 N HCl, 25 °C, 7 days)	No degradation			100.57	100.57	
(2) Alkaline hydrolysis (0.1 N NaOH, 25 °C, 4 h)	DP6—46.61		0.94	32.86	95.35	0.9944
	DP7—0.24	5.45	1.22			0.9997
	DP9—15.62	4.81	1.47			0.9999
	total—62.48					
(3) Peroxide degradation (3% H_2O_2, 25 °C, 24 h)	DP8—0.27	9.66	1.42	97.22	97.50	0.9957
(4) Photolytic degradation (liquid, 1.2 million lux h, 200 W/m^2)	DP1—0.23		0.25	85.00	92.67	0.9999
	DP2—0.35	1.72	0.28			0.9999
	DP3—0.77	7.37	0.66			0.9999
	DP4—1.14	1.47	0.70			0.9998
	DP5—1.10	1.44	0.75			0.9999
	DP7—2.22	3.70	1.20			1.0000
	DP10—1.86	1.10	2.22			0.9997
	total—7.67					
(5) Photolytic degradation (solid, 6 million lux h, 1000 W/m^2)	no degradation			101.39	101.39	
(6) Thermal degradation (100 °C, 7 days)	no degradation			102.18	102.18	

[a]Degradation product.

increasing the time up to 6 million lux h, 1000 W/m^2, no degradation was observed (Figure S2 and Table 1).

From the above results, it can be concluded that a total of 10 DPs were obtained in alkaline, peroxide, and photolytic (liquid) conditions.

Quantification of DPs. The final concentration of 100 μg/mL was injected into the HPLC system in each stress degradation condition. In alkaline hydrolysis, the % degradation values of three DPs DP6, DP7, and DP9 were 46.61% (46.61 μg/mL), 0.24% (0.24 μg/mL), and 15.62% (15.62 μg/mL), respectively. In photolytic degradation, the % degradation values of seven DPs DP1, DP2, DP3, DP4, DP5, DP7, and DP10 were 0.23% (0.23 μg/mL), 0.35% (0.35 μg/mL), 0.77% (0.77 μg/mL), 1.14% (1.14 μg/mL), 1.10% (1.10 μg/mL), 2.22% (2.22 μg/mL), and 1.86% (1.86 μg/mL), respectively.

From the above results, it can be concluded that DP6 and DP9 were found to be the major DPs in alkaline conditions.

LC-ESI-QTOF-MS/MS of PRN and Its DPs.[36−40] The structural characterization of PRN and its DPs was performed using LC-ESI-QTOF-MS/MS. The total ion chromatogram (TIC) was scanned in the range of 50−500 *m/z*. The percentages of DP8 in peroxide degradation was very less (around 0.2%); hence, the product was unable to ionize in MS and further characterization was not possible. Furthermore, the amounts of DP1 and DP2 were observed to be the same (*m/z* 294.8000 Da).

MS/MS Study of PRN (R_t = 15.15 min). The LC-ESI-QTOF-MS/MS spectra of PRN ($[M + H]^+$, *m/z* 482.2000, $C_{27}H_{24}N_5O_4^+$) are shown in Figure S3a. The spectrum shows the product ion at *m/z* 454 (loss of $-N_2$), *m/z* 426 (loss of $-N_2$), *m/z* 346 (loss of $-C_4H_3O_2$ and +2H), *m/z* 294 (loss of $-C_9H_{11}$ and $-CH_3$ from *m/z* 426), *m/z* 266 (loss of $-CH_3OH$), *m/z* 253 (loss of $-C_{10}H_6N_3O_2$ from *m/z* 482), *m/z* 225 (loss of −CO), *m/z* 175 (loss of $-C_6H_5$ from *m/z* 253), *m/z* 147 (loss of $-C_7H_6NO$ from *m/z* 266), *m/z* 133 (loss of $-C_6H_5OH$ from *m/z* 225), *m/z* 119 (loss of $-CH_3$), and *m/z* 91 (loss of $-C_2H_5$) (as shown in Figure S4 and Table 7). The product ion observed at *m/z* 454 and *m/z* 426, which is formed by the loss of $-N_2$, indicates the presence of the tetrazole moiety in PRN. The product ion observed at *m/z* 294, which is formed by the loss of $-C_6H_5CH_2CH_2CH_3$ and $-CH_3$, suggests the presence of the phenyl propyl moiety in PRN. The product ion observed at *m/z* 147, which is formed by the loss of $-NHCOC_6H_5$, indicates the presence of the phenyl amide moiety in PRN.

The LC-ESI-QTOF-MS/MS spectra of PRN ([M-H], *m/z* 480.2000, $C_{27}H_{22}N_5O_4^-$) are shown in Figure S3b. The spectrum shows a product ion at *m/z* 452 (loss of $-N_2$), *m/z* 424 (loss of $-N_2$), *m/z* 290 (loss of $-C_{10}H_{13}O$ and −NH from *m/z* 452), *m/z* 263 (loss of $-CH_2NH_2$), *m/z* 171 (loss of $-C_7H_6NO$ from *m/z* 290), and *m/z* 118 (loss of $-C_{18}H_{11}NO_4$ from *m/z* 424). The product ion observed at *m/z* 452 and *m/z* 424, which is formed by the loss of $-N_2$, indicates the presence of the tetrazole moiety in PRN. The product ion observed at *m/z* 171, which is formed by the loss of $-NHCOC_6H_5$, suggests the presence of the phenyl amide moiety in PRN (as shown in Figures S3a,b and S4a,b and Table 2).

MS/MS, NMR, and FTIR Study of PRN DPs. *DP1 (R_t = 3.87 min) and DP2 (R_t = 4.32 min).* The LC-ESI-QTOF-MS/MS spectra of DP1 and DP2 ($[M + H]^+$, *m/z* 294.8000, $C_{17}H_{14}NO_4^+$) in the photolytic (liquid state) condition are shown in Figure S3c. The precursor ion was 187 Da less than $[M + H]^+$ of PRN due to the loss of $-CHN_4$ and $-C_9H_{11}$ from PRN. The spectrum shows a product ion at *m/z* 147 (loss of $-C_8H_8NO_2$). The product ion observed at *m/z* 147, which is formed by the loss of $-NHCOC_6H_5OCH_3$, indicates the presence of the amide moiety in DP1 and DP2 (as shown in Figures S3c and S4c and Table 2).

DP3 (R_t = 10.13 min). The LC-ESI-QTOF-MS/MS spectra of DP3 ($[M + H]^+$, *m/z* 274.1000, $C_{11}H_8N_5O_4^+$) in the photolytic (liquid state) condition are shown in Figure S3d. The precursor ion was 208 Da less than $[M + H]^+$ of PRN due to the loss of $-C_{16}H_{17}O$ and addition of H_2O from PRN. The spectrum shows a product ion at *m/z* 256 (loss of $-H_2O$) (as shown in Figures S3d and S4d and Table 2).

DP4 (R_t = 10.86 min). The LC-ESI-QTOF-MS/MS spectra of DP4 ([M-H], *m/z* 456.1000, $C_{25}H_{22}N_5O_4^-$) in the photolytic (liquid state) condition is shown in Figure S3e. The precursor ion was 24 Da less than $[M - H]$ of PRN due to the loss of $-C_2H_2$ and addition of +2H from PRN. The spectrum shows a product ion at *m/z* 412 (loss of $-N_3H_3$ and −2H), *m/z* 353 (loss of $-C_6H_9$ and N_2 from *m/z* 456), *m/z* 278 (loss of $-N_2H_4$ and $-C_2H_5OH$), *m/z* 201 (loss of $-C_6H_5$), and *m/z* 147 (loss of $-CONH_2$ and $-CH_3$). The product ion observed at *m/z* 147,

https://doi.org/10.1021/acs.chemrestox.1c00222
Chem. Res. Toxicol. 2022, 35, 1206−1219

Table 2. MS/MS Data and Elemental Composition of PRN and Its DP with Their Product Ions

Sr no.	Name	Molecular weight	Formula	MS/MS fragments
1	PRN	482.2000	$C_{27}H_{24}N_5O_4^+$	454.0500 ($C_{27}H_{24}N_3O_4^+$) 426.1500 ($C_{27}H_{24}NO_4^+$) 346.3000 ($C_{21}H_{16}NO_4^+$) 294.0000 ($C_{17}H_{12}NO_4^+$) 266.1500 ($C_{16}H_{12}NO_3^+$) 253.2000 ($C_{17}H_{17}O_2^+$) 225.1000 ($C_{16}H_{17}O^+$) 174.9000 ($C_{11}H_{11}O_2^+$) 147.0500 ($C_9H_7O_2^+$) 133.1000 ($C_{10}H_{13}^+$) 119.0000 ($C_9H_{11}^+$) 91.1500 ($C_7H_7^+$)
2	PRN	480.2000	$C_{27}H_{22}N_5O_4^-$	452.2500 ($C_{27}H_{22}N_3O_4^-$) 424.3000 ($C_{27}H_{22}NO_4^-$) 290.0000 ($C_{17}H_{11}N_2O_3^-$) 263.2000 ($C_{16}H_{10}NO_3^-$) 171.0000 ($C_{10}H_6NO_2^-$) 118.1000 ($C_9H_{11}^-$)
3	DP1, 2	294.8000	$C_{17}H_{14}NO_4^+$	147.3000 ($C_9H_7O_2^+$)
4	DP3	274.1000	$C_{11}H_8N_5O_4^+$	256.1000 ($C_{11}H_6N_5O_3^+$)
5	DP4	456.1000	$C_{25}H_{22}N_5O_4^-$	411.8500 ($C_{25}H_{19}N_2O_4^-$) 353.5000 ($C_{20}H_{21}N_2O_4^-$) 278.3000 ($C_{17}H_{12}NO_3^-$) 201.5000 ($C_{11}H_8NO_3^-$)
6	DP5	498.2000	$C_{27}H_{24}N_5O_5^+$	147.1500 ($C_9H_7O_2^-$) 470.1500 ($C_{27}H_{27}N_4O_4^+$) 457.0500 ($C_{27}H_{26}N_3O_4^+$) 349.8000 ($C_{21}H_{10}NO_4^+$) 253.1500 ($C_{17}H_{17}O_2^+$) 133.1000 ($C_{10}H_{13}^+$) 119.0500 ($C_9H_{11}^+$)
7	DP6	404.3000	$C_{25}H_{26}NO_4^+$	360.2000 ($C_{24}H_{26}NO_2^+$) 227.1000 ($C_{14}H_{14}NO_2^+$) 210.0500 ($C_{14}H_{12}NO^+$) 151.1000 ($C_8H_{10}NO_2^+$) 134.1000 ($C_8H_8NO^+$)
8	DP7	270.1000	$C_{17}H_{19}O_3^+$	133.1000 ($C_{10}H_{13}^+$) 119.1500 ($C_9H_{11}^+$) 105.3000 ($C_8H_9^+$) 91.0500 ($C_7H_7^+$)
9	DP9	500.1000	$C_{27}H_{26}N_5O_5^+$	426.3000 ($C_{27}H_{26}NO_4^+$) 253.0000 ($C_{17}H_{17}O_2^+$) 119.1000 ($C_9H_{11}^+$) 105.0000 ($C_8H_9^+$) 91.0000 ($C_7H_7^+$)
10	DP10	418.2000	$C_{26}H_{28}NO_4^+$	400.1000 ($C_{26}H_{26}NO_3^+$) 383.2000 ($C_{26}H_{24}NO_2^+$) 252.9000 ($C_{17}H_{17}O_2^+$) 148.1000 ($C_9H_9O_2^+$) 120.9500 ($C_8H_9O^+$)

which is formed by the loss of $-CONH_2$ and $-CH_3$, suggests the presence of the amide moiety in DP4 (as shown in Figures S3e and S4e and Table 2).

DP5 (R_t = 11.58 min). The LC-ESI-QTOF-MS/MS spectra of DP5 ($[M + H]^+$, m/z 498.2000, $C_{27}H_{24}N_5O_5^+$) in the photolytic (liquid state) condition are shown in Figure S3f. The precursor ion was 16 Da more than $[M + H]^+$ of PRN due to the addition of −OH from PRN. The spectrum shows a product ion at m/z 470 (loss of −NH and addition of +3H), m/z 457 (loss of −NH and addition of +3H), m/z 349 (loss of $-C_6H_5$, $-N_2H_4$, and −2H), m/z 253 (loss of $-C_{10}H_9N_3O_2$ from m/z 457), m/z 133 (loss of $-C_7H_4O_2$), and m/z 119 (loss of $-CH_3$). The product ions observed at m/z 470, m/z 457, and m/z 349, which are formed by the loss of −NH, $-NH_3$, and $-N_2H_4$, respectively indicate the presence of the tetrazole moiety in DP5. The product ion observed at m/z 133, which is formed by the loss of $-COC_6H_5O$, suggests the presence of ketone and ether moieties in DP5 (as shown in Figures S3f and S4f and Table 2).

DP6 (R_t = 14.01 min). The LC-ESI-QTOF-MS/MS spectra of DP6 ($[M + H]^+$, m/z 404.3000, $C_{25}H_{26}NO_4^+$) in the alkaline conditions are shown in Figure S3g. The precursor ion was 78 Da less than $[M + H]^+$ of PRN due to the loss of $-C_2HN_4$ and addition of +3H. The spectrum shows product ions at m/z 360 (loss of -2OH and $-CH_3$), m/z 227 (loss of $-C_{10}H_{13}$), m/z 210 (loss of −OH), m/z 151 (loss of $-C_9H_{11}$ and $-C_7H_7$ from m/z 360), and m/z 134 (loss of $-C_6H_5$). The product ion observed at m/z 151, which is formed by the loss of $-CH_2CH_2CH_2CH_2C_6H_5$ and $-CH_2C_6H_5$, indicates the presence of the phenyl butyl moiety in DP6. ^{1}H NMR and ^{13}C NMR spectra of DP6 show the presence of free −OH (20) due to ring-opening caused by breaking of the bond between "O" and "C" of the "oxo pyran" ring system. Furthermore, breaking of the "C═C" bond by removing "C" attached to the tetrazole ring system forms free $-CH_3$ (3). The ^{1}H NMR spectrum of DP6 shows the δ value of free "OH" (1H, 20) at 12.678 ppm and a decrease in the δ value at the third position due to the breaking of the "C═C" bond to form "CH_3" (3H, 3) at 2.499 ppm as compared to PRN. The ^{13}C NMR spectrum of DP6 shows the absence of 1 "C" attached to the tetrazole ring system compared to PRN. FTIR spectrum of DP6 shows the presence of phenolic 'OH'. It shows a sharp stretching frequency at 3440.39 cm^{-1} and medium bending frequency at 1369.21 cm^{-1} compared to PRN. The tetrazole moiety is absent in DP6 hence, it did not show −C═N stretching, −N═N═N stretching, −N−H wagging, and −N−H bending compare to PRN (as shown in Figures S3g, S4g, S5a, S6a,c, and S7a and Tables 2−4).

https://doi.org/10.1021/acs.chemrestox.1c00222
Chem. Res. Toxicol. 2022, 35, 1206−1219

DP7 (R_t = 18.52 min). The LC-ESI-QTOF-MS/MS spectra of DP7 ($[M + H]^+$, m/z 270.1000, $C_{17}H_{19}O_3^+$) in the photolytic (liquid state) condition are shown in Figure S3h. The precursor ion was 212 Da less than $[M + H]^+$ of PRN due to the loss of $-C_{10}H_6N_5O_2$ and addition of −OH from PRN. The spectrum shows product ions at m/z 133 (loss of $-C_7H_5O_3$), m/z 119 (loss of $-CH_3$), m/z 105 (loss of $-CH_3$), and m/z 91 (loss of $-CH_3$). The product ion observed at m/z 134, which is formed by the loss of $-OC_6H_5COOH$, indicates the presence of ether and acid moieties in DP7 (as shown in Figures S3h and S4h, and Table 2).

Table 3. ^{1}H NMR and ^{13}C NMR Assignments for the Procured Impurity and DP9

Position	Procured impurity, δ_H (ppm), multiplicity	DP9, δ_H (ppm), multiplicity	Procured impurity, δ_C (ppm)	DP9, δ_C (ppm)
1	1.728 (4H, m)	1.742 (4H, m)	28.64	28.62
2	2.634−2.681 (2H, t)	2.498−2.648 (2H, t)	35.24	35.22
3	2.499 (3H, s)	3.465 (2H, s)	27.64	40.56
4	4.047 (2H, t)	4.076 (2H, t)	68.04	68.06
5	7.155−7.217 (2H, d)	7.230 (2H, d)	114.60	114.65
6	7.261−7.297 (5H, m)	7.270 (5H, m)	128.77	128.78
7	6.981−7.046 (1H, t)	7.057 (1H, t)	118.93	118.93
8	7.759−7.779 (1H, d)	7.282 (1H, d)	127.56	127.99
9	8.025−8.044 (2H, d)	7.959 (2H, d)	128.73	130.00
10	7.954−7.975 (1H, d)	7.727 (1H, d)	127.96	128.78
11	9.471 (1H, s)	9.557 (1H, s)		
12			142.42	142.44
13			161.95	161.96
14			126.18	126.19
15			165.14	165.37
16			126.52	126.53
17			120.27	121.32
18			154.44	153.84
19			206.12	174.46
20				174.46
21	12.678 (1H, s)	12.404 (1H, s)		

Table 4. FTIR Interpretation of the Procured Impurity

Sr no.	Functional group	Observed wavenumber (cm^{-1})
1	−N−H (stretching, medium)	3690.12
2	−O−H (stretching, strong)	3440.39
3	−O−H (bending, medium)	1369.21
4	−C−N (stretching, strong) aromatic amine	1243.86
5	−C═O (stretching, strong)	1669.09
6	−C−O(H) (stretching, strong)	1145.51
7	−C−H aliphatic (stretching, medium)	2939.95
8	−C−H aromatic (stretching)	3025.76

DP9 (R_t = 21.94 min). The LC-ESI-QTOF-MS/MS spectra of DP9 ($[M + H]^+$, m/z 500.1000, $C_{27}H_{26}N_5O_5^+$) in the alkaline condition are shown in Figure S3i. The precursor ion was 18 Da more than $[M + H]^+$ of PRN due to the addition of the "O" atom and H^+ atom from PRN. The spectrum shows product ions at m/z 426 (loss of $-N_4$), m/z 253 (loss of $-C_{10}H_7NO_2$), m/z 119 (loss of $-C_8H_7O_2$), m/z 105 (loss of $-CH_3$), and m/z 91 (loss of $-CH_3$). The product ion observed at m/z 426, which is formed by the loss of $-N_4$, indicates the presence of the tetrazole moiety in DP9. The product ion observed at m/z 253, formed by the loss of $-NHC_6H_5COCH{=}CH(OH)CH_3$, indicates the presence of the 4-oxo benzopyran moiety in DP9. The product ion observed at m/z 119, which is formed by the loss of $-COC_6H_5OCH_3$, indicates the presence of phenyl ketone and ether moieties in DP9 (as shown in Table 7). The ^{1}H NMR and ^{13}C NMR spectra of DP9 show the presence of free −OH (21) due to ring-opening caused by breaking the bond between "O" and "C" of the "oxo pyran" ring system. Furthermore, the presence of "═O" (20) is caused by the breaking of the "C═C" bond to the "C−C" bond (3). The ^{1}H NMR spectrum of DP9 shows the δ value of free "OH" (1H, 21) at 12.404 ppm and a decrease in the δ value at the third position due to the breaking of the "C═C" bond to form "CH_2" (2H, 3) at 3.465 ppm as compared to PRN. The ^{13}C NMR spectrum of DP9 shows the δ value of "═O" (20) at 174.46 ppm compared to PRN. FTIR spectrum of DP9 shows the presence of phenolic 'OH'. It shows a sharp stretching frequency at 3447.13 cm^{-1} and medium bending frequency at 1359.57 cm^{-1} compared to PRN (as shown in Figures S3i, S4i, S5b, S6b,d, and S7b and Tables 2, 3, and 5).

Table 5. FTIR Interpretation of DP9

Sr no.	Functional group	Observed wavenumber (cm^{-1})
1	−N−H (stretching, medium, 2 bands) amide	3600.45
2	−O−H (stretching, strong)	3448.1
3	−O−H (bending, medium)	1358.6
4	−C−N (stretching, strong) aromatic amine	1235.18
5	−N−H (wagging) 1° amine	718.35
6	−N−H (bending, medium)	1637.27
7	−C═O (stretching, strong) 2° amide	1673.91
8	−C═N (stretching)	1542.77
9	−-N═N−N (stretching)	2137.71
10	−C−O(H) (stretching, strong)	1071.26
11	−C−H aliphatic (stretching, medium)	2940.91
12	−C−H aromatic (stretching)	3031.55

DP10 (R_t = 34.18 min). The LC-ESI-QTOF-MS/MS spectra of DP10 ($[M + H]^+$, m/z 418.2000, $C_{26}H_{28}NO_4^+$) in the photolytic (liquid state) condition is shown in Figure S3j. The precursor ion was 64 Da less than $[M + H]^+$ of PRN due to the loss of $-CHN_4$ and addition of +4H from PRN. The spectrum shows product ions at m/z 400 (loss of $-H_2O$), m/z 383 (loss of −OH), m/z 253 (loss of $-C_9H_7N$), m/z 148 (loss of $-C_8H_9$), and m/z 121 (loss of −CO). The product ion observed at m/z 400, which is formed by the loss of $-H_2O$, indicates the presence of the alcohol moiety in DP10. The product ion observed at m/z 148, which is formed by the loss of $-C_8H_9$, indicates the presence of the phenyl ethyl moiety in DP10 (as shown in Figures S3j and S4j and Table 2).

Proposed Degradation Pathway of the Drug.[41] The mechanism of the degradation pathway was based on hydrolysis degradation (deamination, demethylation, and hydration reaction) and photolytic degradation (deamination, hydration, dealkylation, dephenylation, and de-ether reaction). In alkaline conditions, two DPs were obtained, namely, DP6 [loss of the $-C_2HN_4$ group (deamination and demethylation), followed by the addition of +3H (protonation)] and DP9 [addition of the

https://doi.org/10.1021/acs.chemrestox.1c00222
Chem. Res. Toxicol. 2022, 35, 1206−1219

Table 6. In Silico Toxicity Prediction of PRN and Its DP by Using admetSAR Software

		PRN and its degradation products								
ADMET properties	Identifier	PRN	DP1, 2	DP3	DP4	DP5	DP6	DP7	DP9	DP10
Solubility	log *S*	−3.525	−3.397	−3.652	−3.492	−3.257	−3.447	−3.25	−2.91	−3.444
Plasma protein binding		1.114 (100%)	0.921 (100%)	0.951 (100%)	0.98 (100%)	1.22 (100%)	1.069 (100%)	0.896 (100%)	1.198 (100%)	0.898 (100%)
Lipophilicity	*A* log *P*	4.63	2.50	0.23	5.46	4.34	5.25	3.79	4.62	5.64
Human intestinal absorption		0.9564 (+)	0.8127 (+)	0.8929 (+)	0.9346 (+)	0.9350 (+)	0.9866 (+)	0.9925 (+)	0.9678 (+)	0.9866 (+)
Permeability		0.9743 (+)	0.9732 (+)	0.9726 (+)	0.9694 (+)	0.9739 (+)	0.8966 (+)	0.8965 (+)	0.9685 (+)	0.8924 (+)
Human oral bioavailability		0.5714 (−)	0.5429 (+)	0.5143 (+)	0.5000 (−)	0.5000 (−)	0.5429 (−)	0.6571 (−)	0.5286 (−)	0.5429 (+)
Transporters	OATP2B1 inhibitor	0.8555 (−)	1.0000 (−)	1.0000 (−)	1.0000 (−)	0.8569 (−)	1.0000 (−)	1.0000 (−)	0.5680 (−)	1.0000 (−)
	OATP1B1 inhibitor	0.8646 (+)	0.9208 (+)	0.9133 (+)	0.8984 (+)	0.8834 (+)	0.8531 (+)	0.8968 (+)	0.8531 (+)	0.8436 (+)
	OATP1B3 inhibitor	0.9327 (+)	0.9761 (+)	0.9375 (+)	0.9431 (+)	0.9256 (+)	0.9364 (+)	0.9483 (+)	0.9355 (+)	0.9422 (+)
	MATE1 inhibitor	0.9409 (−)	0.9600 (−)	0.8600 (−)	0.9400 (−)	0.9200 (−)	0.9200 (−)	0.7686 (−)	0.9209 (−)	0.9200 (−)
	OCT2 inhibitor	0.6071 (−)	1.0000 (−)	0.9500 (−)	0.8000 (−)	0.5859 (−)	0.8750 (−)	0.7750 (−)	0.8000 (−)	0.9000 (−)
	BSEP inhibitor	0.8266 (+)	0.5303 (−)	0.9171 (−)	0.6824 (+)	0.7570 (+)	0.5668 (−)	0.6855 (+)	0.4630 (−)	0.5000 (−)
	P-gp inhibitor	0.9085 (+)	0.6191 (−)	0.9183 (−)	0.8735 (+)	0.8746 (+)	0.8805 (+)	0.9426 (+)	0.8813 (+)	0.8978 (+)
	P-gp substrate	0.6939 (+)	0.7283 (−)	0.5207 (+)	0.6242 (+)	0.6760 (+)	0.6338 (+)	0.6003 (+)	0.6388 (+)	0.6211 (+)
CYP substrates	CYP3A4 substrate	0.6886 (+)	0.5614 (+)	0.5456 (+)	0.6500 (+)	0.7031 (+)	0.6452 (+)	0.6301 (+)	0.6717 (+)	0.6394 (+)
	CYP2C9 substrate	1.0000 (−)	1.0000 (−)	1.0000 (−)	0.8046 (−)	1.0000 (−)	0.8097 (−)	0.8019 (−)	0.5923 (+)	0.8097 (−)
	CYP2D6 substrate	0.8387 (−)	0.8504 (−)	0.8630 (−)	0.8535 (−)	0.8570 (−)	0.8271 (−)	0.8076 (−)	0.8404 (−)	0.8271 (−)
CYP inhibition	CYP3A4 inhibitor	0.5679 (−)	0.8321 (−)	0.7093 (−)	0.8677 (−)	0.6004 (+)	0.8891 (−)	0.8042 (+)	0.8066 (−)	0.9090 (−)
	CYP2C9 inhibitor	0.5597 (−)	0.6878 (−)	0.6912 (−)	0.5901 (−)	0.5273 (+)	0.6061 (−)	0.5067 (−)	0.8154 (−)	0.6508 (−)
	CYP2C19 inhibitor	0.5194 (−)	0.8831 (−)	0.7610 (−)	0.5313 (+)	0.5690 (−)	0.7163 (+)	0.7899 (+)	0.7226 (−)	0.8345 (+)
	CYP2D6 inhibitor	0.8714 (−)	0.8648 (−)	0.7878 (−)	0.8141 (−)	0.8642 (−)	0.8700 (−)	0.9003 (−)	0.8888 (−)	0.8406 (−)
	CYP1A2 inhibitor	0.7009 (−)	0.8155 (+)	0.7195 (−)	0.5000 (−)	0.6890 (−)	0.6268 (−)	0.8360 (+)	0.7410 (−)	0.5709 (−)
Sensitization	Eye corrosion	0.9886 (−)	0.9858 (−)	0.9846 (−)	0.9867 (−)	0.9868 (−)	0.9946 (−)	0.9804 (−)	0.9887 (−)	0.9941 (−)
	Eye irritation	0.9540 (−)	0.7049 (+)	0.8017 (−)	0.9534 (−)	0.9545 (−)	0.8687 (−)	0.9124 (+)	0.9339 (−)	0.8926 (−)
Receptor binding	Estrogen	0.7728 (+)	0.7623 (+)	0.6896 (+)	0.8303 (+)	0.7651 (+)	0.7737 (+)	0.6805 (+)	0.7638 (+)	0.7219 (+)
	Androgen	0.9314 (+)	0.8835 (+)	0.6506 (+)	0.9685 (+)	0.9426 (+)	0.9246 (+)	0.9303 (+)	0.8047 (+)	0.9015 (+)
	Thyroid	0.6391 (+)	0.6403 (+)	0.5848 (+)	0.6038 (+)	0.6383 (+)	0.5750 (+)	0.7149 (+)	0.5154 (+)	0.5167 (+)
	Glucocorticoid	0.7128 (+)	0.7592 (+)	0.5628 (+)	0.7736 (+)	0.7017 (+)	0.6633 (+)	0.6436 (+)	0.6932 (+)	0.7366 (+)
Toxicity endpoint	Ames mutagenicity	0.5700 (−)	0.5500 (+)	0.6300 (−)	0.5500 (−)	0.5500 (−)	0.6400 (−)	0.6300 (−)	0.5200 (−)	0.6300 (−)
	Micronuclear toxicity	0.9000 (+)	0.9000 (+)	0.9700 (+)	0.8100 (+)	0.9700 (+)	0.7400 (+)	0.8197 (−)	0.8400 (+)	0.7400 (+)
	Carcinogenicity	0.9503 (−)	0.8534 (−)	0.9000 (−)	0.9360 (−)	0.9217 (−)	0.8303 (−)	0.9143 (−)	0.9217 (−)	0.8303 (−)
	Hepatotoxicity	0.8000 (+)	0.9250 (+)	0.9000 (+)	0.8000 (+)	0.8250 (+)	0.8250 (+)	0.7250 (+)	0.8250 (+)	0.8000 (+)
	Acute oral toxicity	2.077 kg/mol	2.387 kg/mol	1.811 kg/mol	2.729 kg/mol	2.42 kg/mol	1.873 kg/mol	1.863 kg/mol	2.372 kg/mol	1.59 kg/mol
		0.7272 (III)	0.7130 (III)	0.6207 (III)	0.7081 (III)	07170 (III)	0.8159 (III)	0.6666 (III)	0.7307 (III)	0.8133 (III)
	Aquatic toxicity	0.6956 (+)	0.8601 (+)	0.8693 (+)	0.4355 (−)	0.8426 (+)	0.9535 (+)	0.9850 (+)	0.8210 (+)	0.9707 (+)

https://doi.org/10.1021/acs.chemrestox.1c00222
Chem. Res. Toxicol. 2022, 35, 1206−1219

Table 7. In Silico Toxicity Prediction of PRN and Its DP by Using QSAR Toolbox Software

	PRN and its degradation products								
ADMET properties	PRN	DP1, 2	DP3	DP4	DP5	DP6	DP7	DP9	DP10
Skin irritation/corrosion	Ketone	Ketone	Ketone	Ketone	Ketone	Ketone		Ketone	Ketone
Toxic hazard classification by Cramer	High (class III)	High (class III)	High (class III)	High (class III)	High (class III)	High (class III)	High (class III)	High (class III)	High (class III)
Oncological classification			Carbamate type compound			Phenol type compound		Phenol type compound	Phenol type compound
In vitro mutagenicity (Ames test)		α,β unsaturated carbonyls		α,β unsaturated carbonyls					
Carcinogenicity		α,β unsaturated carbonyls		α,β unsaturated carbonyls					
In vivo mutagenicity (micronucleus)	H-acceptor−path3−H-acceptor	α,β unsaturated carbonyls	H-acceptor−path3−H-acceptor	α,β unsaturated carbonyls	H-acceptor−path3−H-acceptor	H-acceptor−path3−H-acceptor		H-acceptor−path3−H-acceptor	H-acceptor−path3−H-acceptor
Hepatotoxicity	Tamoxifen alert	Bromfenac alert		Tamoxifen alert		Mefenamic acid alert	3-methyl-cholantrene alert		Oxyphen-butazone alert
Aquatic toxicity classification by ECOSAR	Amides	Amides	Vinyl/allyl ethers	Aliphatic amines	Amides	Amides		Amides	Amides
	Vinyl/allyl ethers	Vinyl/allyl ethers	Vinyl/allyl ketones	Amides	Vinyl/allyl ethers	Phenol amines		Phenol amines	Phenol amines
	Vinyl/allyl ketones	Vinyl/allyl ketones		Vinyl/allyl ethers	Vinyl/allyl ketones	Phenols		Phenols	Phenols
				Vinyl/allyl ketones				Diketones	

https://doi.org/10.1021/acs.chemrestox.1c00222
Chem. Res. Toxicol. 2022, 35, 1206−1219

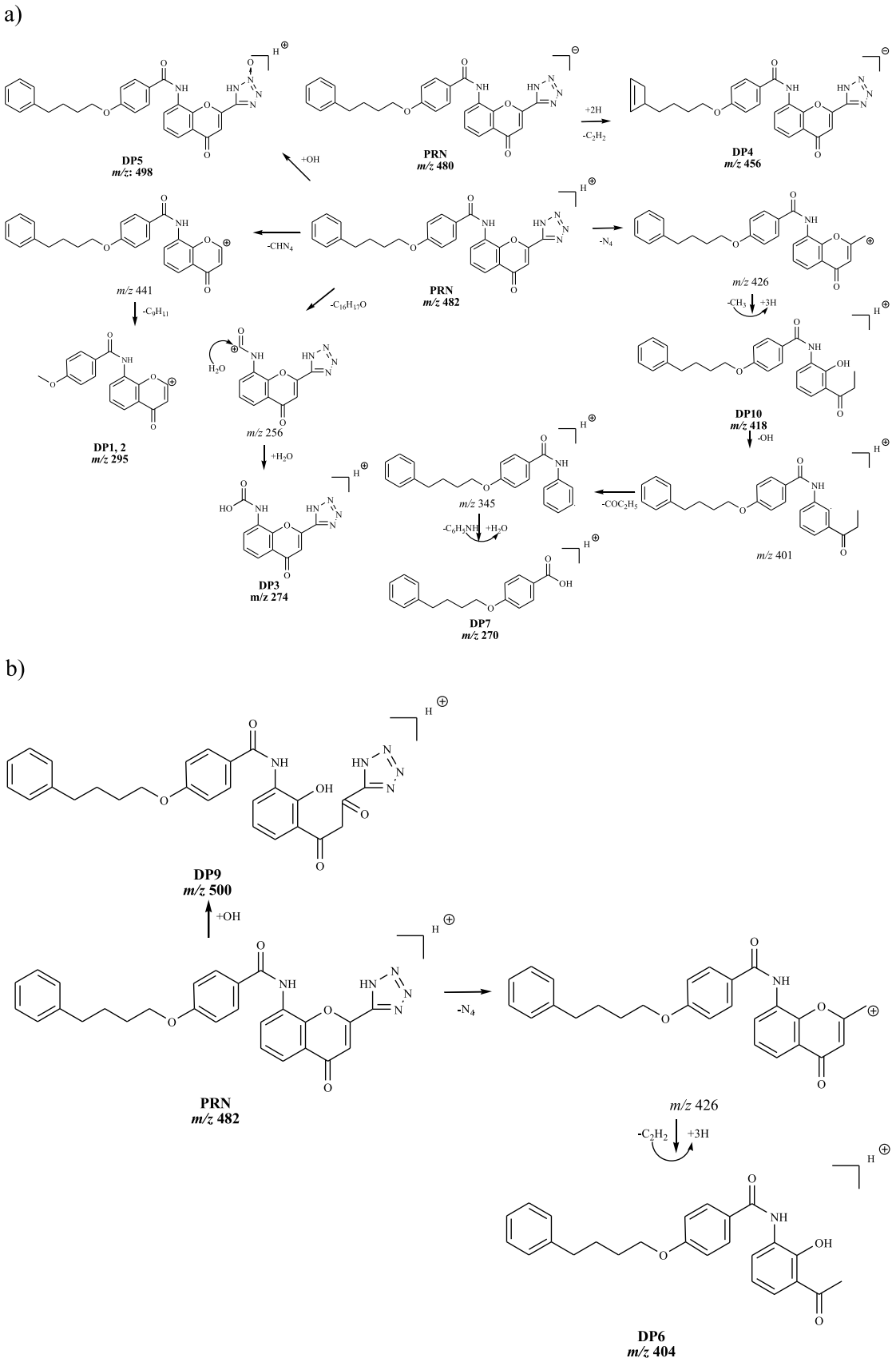

Figure 1. Proposed degradation mechanism of (a) photolytic degradation and (b) alkaline degradation.

−OH group (hydration)]. In the photolytic liquid-state condition, 10 DPs were obtained, namely, DP1, DP2 [loss of the $-CHN_4$ group (deamination) and loss of the $-C_9H_{11}$ group (de aryl alkyl)], DP3 [loss of the $-C_{16}H_{17}O$ group (de aryl alkyl

https://doi.org/10.1021/acs.chemrestox.1c00222
Chem. Res. Toxicol. 2022, 35, 1206−1219

ether), followed by the addition of $-H_2O$ (hydration)], DP4 [loss of $-C_2H_2$ (ethylene) (dealkylation), followed by the addition of the +2H (proton) group (protonation)], DP5 [addition of the −OH group (hydration)], DP7 [loss of the $-C_{10}H_6N_5O_2$ group (deamination and removal of the benzopyran ring system), followed by the addition of the −OH (hydration) Michael addition reaction], and DP10 [loss of the $-CHN_4$ group (deamination), followed by the addition of +3H (protonation)] (details are shown in Figure 1).

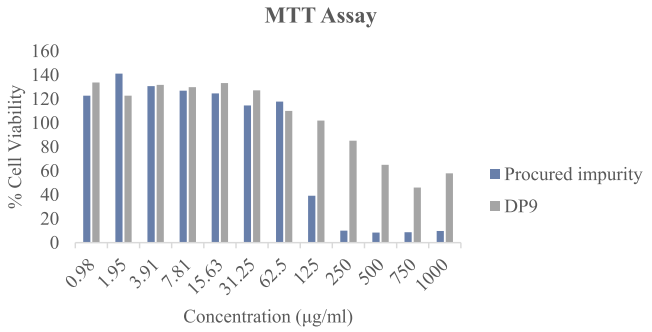

Figure 2. % cell viability vs concentration (μg/mL) plot of the procured impurity and DP9 from the MTT assay using an A549 cell line.

Method Validation. The system suitability study was passed as the % RSD was found to be less than 2% in all four parameters (mobile phase composition, pH, flow rate, and temperature) (Table S1). The calibration curve showed a good linear relationship, and the correlation coefficient (r) value was 0.9999. The regression equation was $y = 246{,}55x + 557{,}495$ (as shown in Figure S8 and Table S2). The LOD and LOQ were 2.00 and 6.09 μg/mL, respectively (Table S2). The % RSD values of intra-day and inter-day precision were found to be 0.06−0.94 and 0.25−0.88%, respectively, which are less than 2%; hence, the method was found to be precise (Table S2). The mean % recovery was found to be in the range of 98.83−100.73%, where the acceptable range is between 98 and 102%; hence, the method was found to be accurate (Table S2). The % RSD of the area, tailing factor, and NTP was found to be 0.11−1.00, 0.99−1.60, and 0.16−1.71%, respectively, in all four parameters: mobile phase composition, pH, flow rate, and wavelength, which are less than 2%; hence, the method was found to be robust (Table S3). All the peaks were well-separated (resolution more than 1.5) without any significant interference or co-elution between the drug peak and the degradation peaks (Figures S2 and S3); hence, the method was found to be specific.

Isolation of DP9. The isolation of the alkaline DP (DP9) was performed by preparative HPLC. The chromatographic separation was achieved using a Waters Xbridge C18 column (250 × 19 mm, 5 μ) with a mobile phase consisted of ammonium format (50 mM), pH 4, with formic acid: ACN (50:50, v/v) in the isocratic mode at a flow rate of 17 mL/min. The chromatograms were monitored at 260 nm wavelength (λ). The injection volume was 5 mL. PRN with a concentration of 5000 μg/mL with DMSO/ACN (1:1) was degraded using 0.1 N NaOH at 25 °C for 6 h and neutralized with 0.1 N HCl. The final solution was diluted with ACN to obtain a 1000 μg/mL solution and evaporated at 65 °C using a rotary evaporator to remove DMSO as it interferes in preparative HPLC, so the final solution volume of 100 mL was used for preparative HPLC. The different fractions were collected, and each fraction's purity was checked using LC−MS (Waters, Milford, MA, USA) to obtain >95% pure DP. The fractions were extracted with water and ethyl acetate to remove the buffer solution, concentrated at 40 °C in a rotary evaporator, and further lyophilized to obtain a solid DP. The isolated sample was characterized using MS/MS, ^{1}H NMR, and ^{13}C NMR.

The isolation of alkaline DP (DP6) was tried. Several attempts were made, but it was difficult to isolate. Hence, the mass of DP6 was confirmed using LC-ESI-QTOF-MS/MS.

The percentage degradation was less than 5% in each DP in the photolytic condition; hence, the isolation was not performed in the photolytic degradation condition.

In Silico Toxicity Study. *Using admetSAR Software (Version 2.0).* The solubility (log S) was predicted to be lower in DP9 than in PRN and other DPs. Plasma protein binding was predicted to be 100% in PRN and its DPs. The lipophilicity (A log P) was predicted to be higher in DP4, DP6, and DP10 but predicted to be lower in other DPs than in PRN. The permeability was predicted to be higher in PRN than in its DPs. The human intestinal absorption was predicted to be higher in DP6, DP7, DP9, and DP10 but predicted to be lower in other DPs than in PRN. The human oral bioavailability of PRN and its DPs was predicted to be poor except for DP1, DP2, DP3, and DP10. In transporters, PRN and its DPs were the predicted inhibitors of OATP1B1 and OATP1B3; PRN, DP4, DP5, and DP7 were predicted inhibitors of bile salt export pump (BSEP); PRN, DP4, DP5, DP6, DP7, DP9, and DP10 were predicted inhibitors of P-glycoprotein; and PRN, DP3, DP4, DP5, DP6, DP7, DP9, and DP10 were predicted substrates of P-glycoprotein. PRN and its DPs were predicted substrates of CYP3A4. DP5 and DP7 were predicted inhibitors of CYP3A4. DP5 was a predicted inhibitor of CYP2C9. DP4, DP6, DP7, and DP10 were predicted inhibitors of CYP2C19. DP1, DP2, and DP7 were predicted inhibitors of CYP1A2. DP1, DP2, and DP7 were predicted irritants to the eye. PRN and its DPs were predicted to bind to thyroid receptors except DP1 and DP2. PRN and its DPs were predicted to bind to androgen and glucocorticoid receptors. DP1 and DP2 were predicted to be mutagenic toxic according to the Ames mutagenicity test, while PRN and its DPs were predicted to be mutagenic toxic according to the micronucleus toxicity test except DP7. None was predicted to be carcinogenic. PRN and its DPs were predicted to be hepatotoxic. PRN and its DPs were predicted to be class-III acute oral toxic. DP1, DP2, DP3, DP5, DP6, DP7, DP9, and DP10 were predicted to be aquatic toxic.

Using QSAR Toolbox Software. PRN and its DPs were predicted to show irritation/corrosion to the skin except for DP7. PRN and its DPs were predicted to show high (class-III) toxicity as per the toxic hazard classification by Cramer. DP3, DP6, DP9, and DP10 were analyzed according to the oncological classification. DP1, DP2, and DP4 were predicted to be mutagenic with in vitro mutagenicity (AMES test). DP1, DP2, and DP4 were predicted to be carcinogens. PRN and its DPs were predicted to be mutagenic with in vivo mutagenicity (micronucleus test) except DP7. PRN, DP1, DP2, DP4, DP6, DP7, and DP10 were predicted to be hepatotoxic. PRN and its DPs were predicted to be aquatic toxic according to the ECOSAR aquatic toxicity classification.

The ketone group is responsible for skin irritation/corrosion in PRN and its DPs except for DP7. DP3 was predicted to be a carbamate type compound; and DP6, DP9, and DP10 were predicted to be phenol type compounds as per the oncological classification. The α,β-unsaturated carbonyl group is responsible for mutagenicity and carcinogenicity in DP1, DP2, and DP4.

https://doi.org/10.1021/acs.chemrestox.1c00222
Chem. Res. Toxicol. 2022, 35, 1206−1219

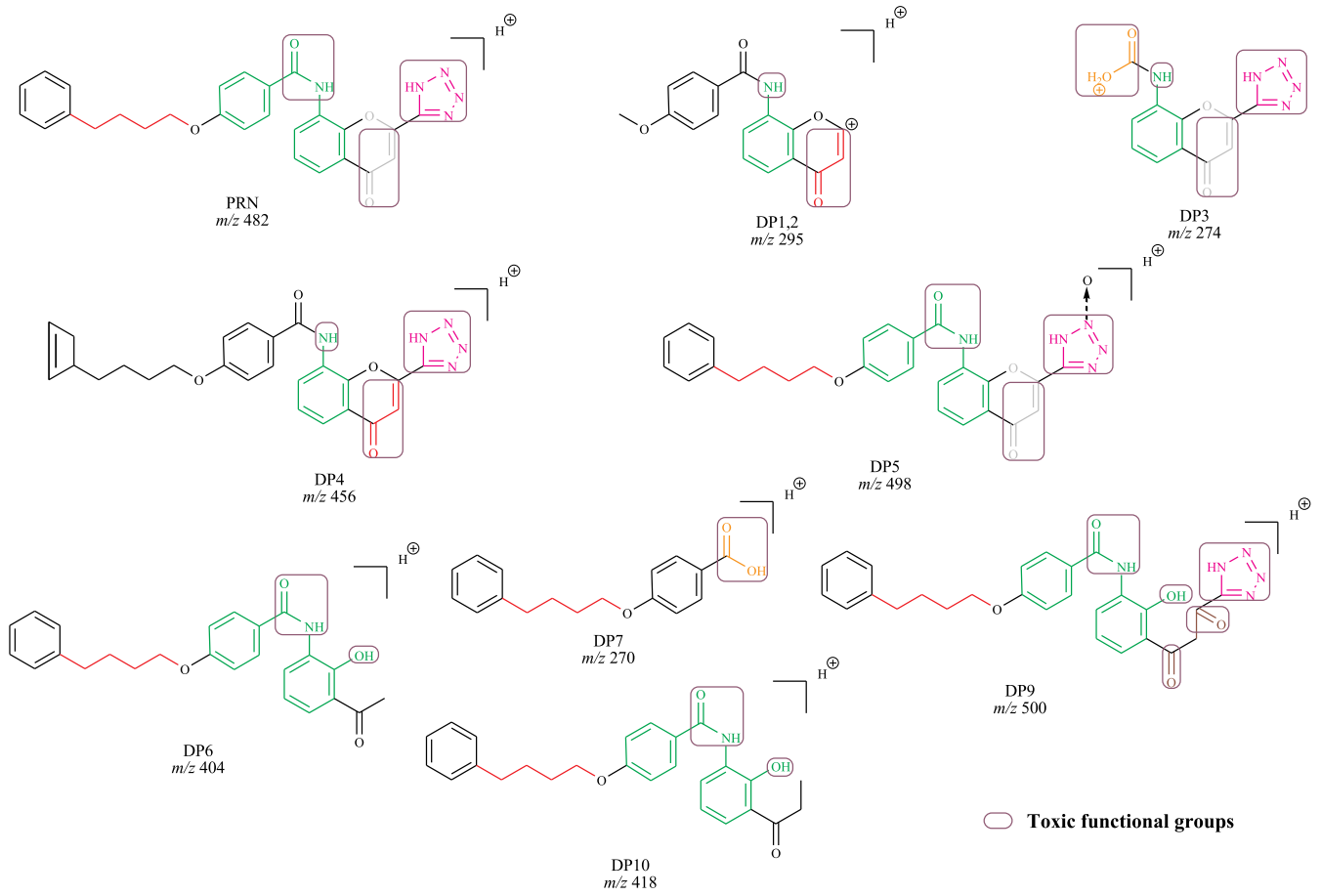

Figure 3. Schematic representation of toxic functional groups of PRN and its DPs.

The H-acceptor−path3−H-acceptor group is responsible for micronucleus toxicity in PRN, DP3, DP5, DP6, DP7, DP9, and DP10. The aromatic amine group is responsible for hepatotoxicity in PRN and its DPs except for DP7. The aliphatic amine group is responsible for hepatotoxicity in DP4. The tetrazole group is also responsible for hepatotoxicity in PRN, DP3, DP5, and DP9. The carboxylic acid group is responsible for hepatotoxicity in DP3 and DP7. PRN and DP4 were predicted to be hepatotoxic, similar to tamoxifen. DP1 and DP2 were predicted hepatotoxicity line bromfenac. DP6 was predicted to be hepatotoxic, similar to mefenamic acid. DP7 was predicted to be hepatotoxic, similar to 3-methylcholantrene. DP10 was predicted to be hepatotoxic, similar to oxyphenbutazone. The aromatic amide group is responsible for fish aquatic toxicity in PRN, DP1, DP2, DP5, DP6, DP9, and DP10. The vinyl/allyl ether and vinyl/allyl ketone groups are responsible for fish aquatic toxicity in PRN, DP1, DP2, DP3, and DP5. The phenol amine and phenol groups are responsible for fish aquatic toxicity in DP6, DP9, and DP10. The diketone group is responsible for fish aquatic toxicity in DP9 (Figure 3 and Tables 6 and 7).

From the above information, we can conclude that DP1, DP2, DP6, and DP10 were predicted to be mutagenic, hepatotoxic, and aquatic toxic. Thus, it may be a risk to human health, and a human adverse event may be observed.

In Vitro Cytotoxicity Study. The in vitro cytotoxicity study of PRN DPs (DP9) and the procured impurity was performed on the A549 cell line using an MTT assay. The result stated that if the % viability was reduced to <70%, it has cytotoxic potential. The procured impurity and DP9 were observed to have 39.2 and 65% cell viabilities at 125 and 500 μg/mL, respectively. The procured impurity and DP9 were observed to be cytotoxic at concentrations above 62.5 and 250 μg/mL, respectively. Hence, the impurities in high concentrations need to be controlled because human adverse events may be observed (Figure 2 and Tables S4 and S5).

CONCLUSIONS

A simple, specific, linear, accurate, precise, robust, sensitive, and stability-indicating method was developed. The forced degradation study was performed as per ICH Q1A (R2) and ICH Q1B guidelines using LC−MS. The alkaline hydrolysis of PRN yields a total of three DPs (DP6, DP7, and DP9). The photolytic (liquid state) degradation yields seven DPs (DP1, DP2, DP3, DP4, DP5, DP7, and DP10). The peroxide degradation yields one DP (DP8). The drug was found to be stable in acidic, photolytic (solid), and thermal degradation. The validation was performed as per ICH Q2 (R1) guidelines. The structure of the DPs was characterized using LC-ESI-QTOF-MS/MS, and a total of eight novel DPs were found, namely, DP1, DP3, DP4, DP5, DP6, DP7, DP9, and DP10. The detailed degradation pathway and the mechanism were analyzed. The isolation of DP9 was carried out using preparative HPLC, and DP9 was found to be 96.8% pure. The characterization of isolated DP9 and the procured impurity was performed using MS/MS, ^{1}H NMR, ^{13}C NMR, and FTIR spectroscopy. The in silico toxicity study was conducted to predict the toxicity of PRN and its DPs using admetSAR software version 2.0 and the QSAR toolbox. DP1, DP2, and DP4 were predicted to be mutagenic toxic using

https://doi.org/10.1021/acs.chemrestox.1c00222
Chem. Res. Toxicol. 2022, 35, 1206−1219

the Ames mutagenicity test using the QSAR toolbox, while PRN and its DPs were predicted to be mutagenic toxic using the micronucleus toxicity test except for DP7. DP1, DP2, and DP4 were predicted to be carcinogenic using the QSAR toolbox. PRN, DP1, DP2, DP4, DP6, DP7, and DP10 were predicted to be hepatotoxic. PRN and its DPs were predicted to show class-III acute oral toxicity. PRN, DP1, DP2, DP3, DP5, DP6, DP7, DP9, and DP10 were predicted to be aquatic toxic. The in vitro toxicity study of the procured impurity and DP9 was performed using an MTT assay using an A549 cell line, and both were observed to be cytotoxic at higher concentrations. Hence, it needs to control the impurities in high concentrations. The combination of characterization and toxicity study played an essential role in analyzing the PRN DPs, which could have a critical impact on the quality, safety, and toxicity of PRN. We can conclude that the proposed method can be used for the stability-indicating method of PRN, and the drug should be stored at 25 °C and kept away from the exposure of light. Furthermore, DP1, DP2, DP6, and DP10 were found to be hepatotoxic, mutagenic using the micronucleus test, and aquatic toxic, and human adverse events may be observed; hence, it is necessary to control these impurities below the toxic level.

■ ASSOCIATED CONTENT

Supporting Information

The Supporting Information is available free of charge at https://pubs.acs.org/doi/10.1021/acs.chemrestox.1c00222.

System suitability parameters of PRN; linearity, precision, and accuracy parameters of PRN at 230 nm; robustness parameters of PRN; in vitro cytotoxicity of the procured impurity using an MTT assay; in vitro cytotoxicity of DP9 using an MTT assay; optimized chromatogram of PRN at 230 nm; chromatogram of PRN and its DPs; ESI-QTOF-MS/MS spectrum; proposed fragmentation pathway; chemical structure; ^{1}H NMR and ^{13}C NMR spectra; FTIR spectrum; and linearity chromatogram of PRN at 230 nm (PDF)

■ AUTHOR INFORMATION

Corresponding Author

Charmy S. Kothari − *Department of Pharmaceutical Analysis, Institute of Pharmacy, Nirma University, Ahmedabad 382 481 Gujarat, India;* orcid.org/0000-0001-5072-1330; Phone: +91 9898617612; Email: charmyshah@gmail.com, charmy.kothari@nirmauni.ac.in

Author

Krunal J. Prajapati − *Department of Pharmaceutical Analysis, Institute of Pharmacy, Nirma University, Ahmedabad 382 481 Gujarat, India*

Complete contact information is available at: https://pubs.acs.org/10.1021/acs.chemrestox.1c00222

Funding

The authors received no financial support for this research.

Notes

The authors declare no competing financial interest.

■ ACKNOWLEDGMENTS

The authors are highly thankful to the Indian Council of Medical Research (ICMR) for providing a Senior Research Fellowship (SRF). We want to thank the Institute of Pharmacy, Nirma University, Ahmedabad, for providing the facility to carry out this research work. We want to thank Saurashtra University, Rajkot, for the LC−MS characterization. We want to thank K.M. Pharma, Ahmedabad, for the isolation by preparative HPLC. We want to thank Reliance Life Sciences Pvt. Ltd., Mumbai, for the in vitro toxicity study.

■ ABBREVIATIONS

PRN, Pranlukast hydrate; CysLT1, cysteinyl leukotriene receptor antagonist; PDA, photodiode array; ICH, International Conference on Harmonization; LC-ESI-QTOF-MS/MS, liquid chromatography−electron spray ionization−quadrupole time of flight−tandem mass spectrometry; DP, degradation product; NMR, nuclear magnetic resonance spectrometry; MTT, 3-(4,5-dimethylthiazol-2-yl)-2,5-diphenyl tetrazolium bromide; JP, Japanese pharmacopoeia; API, active pharmaceutical ingredient; AR, analytical grade; HCl, hydrochloric acid; NaOH, sodium hydroxide; H_2O_2, hydrogen peroxide; DL, desolvation temperature; DMSO, dimethyl sulfoxide; DMF, dimethylformamide; ACN, acetonitrile; LOD, limit of detection; LOQ, limit of quantification; NTP, number of theoretical plates; % RSD, % relative standard deviation; ADMET, absorption, distribution, metabolism, excretion, and toxicity; CYP, cytochrome P450; PBS, phosphate-buffered saline; FBS, fetal bovine serum; DMEM, Dulbecco's modified Eagle's medium; ELISA, enzyme-linked immune sorbent assay; NC, negative control; TIC, total ion chromatogram; OATP, organic anion transporter; BSEP, bile salt export pump

■ SYMBOLS

mm	millimeter
μ	micron
mM	millimolar
v/v	volume by volume
mL/min	milliliter per minute
nm	nanometer
μg/mL	microgram per milliliter
w/w	weight by weight
λ	wavelength
°C	°celsius
L/min	liter per minute
R.H.	relative humidity
h	hour
W/m^2	watt per meter square
t_R	retention time
μAU	microampere
N	normality
m/z	mass to charge ratio
δ	chemical shift
log S	solubility
A log P	lipophilicity

■ REFERENCES

(1) Marchese, A.; McHugh, C.; Kehler, J.; Bi, H. Determination of and its metabolites in pranlukast human plasma by LC/MS/MS with PROSPEKT on-line solid-phase extraction. *J. Mass Spectrom.* **1998**, *33*, 1071−1079.

(2) Baek, M.-K.; Lee, J.-H.; Cho, Y.-H.; Kim, H.-H.; Lee, G.-H. Self-microemulsifying drug-delivery system for improved oral bioavailability of pranlukasthemihydrate: preparation and evaluation. *Int. J. Nanomed.* **2013**, *8*, 167−176.

(3) Hao, Y.; Wang, L.; Li, J.; Liu, N.; Feng, J.; Zhao, M.; Zhang, X. Enhancement of solubility, transport across madin-darby canine kidney

monolayers and oralabsorption of pranlukast through preparation of a pranlukast-phospholipid complex. *J. Biomed. Nanotechnol.* **2015**, *11*, 469−477.
(4) Wang, L.; Hao, Y.; Liu, N.; Ma, M.; Yin, Z.; Zhang, X. Enhance the dissolution rate and oral bioavailability of pranlukast by preparing nanosuspensions with high pressure homogenizing method. *Drug Dev. Ind. Pharm.* **2012**, *38*, 1381−1389.
(5) Yoneda, K.; Matsumoto, I.; Sutoh, F.; Higashi, R.; Nunoya, K.-i.; Nakade, S.; Miyata, Y.; Ogawa, M. In vitro metabolism and inhibitory effects of pranlukast in human liver microsomes. *Biol. Pharm. Bull.* **2009**, *32*, 688−693.
(6) Shankar, G.; Borkar, R. M.; Udutha, S.; Kanakaraju, M.; Charan, G. S.; Misra, S.; Srinivas, R. Identification and structural characterization of stress degradation products of omeprazole using Q-TOF-LC-ESI-MS/MS and NMR experiments: Evaluation of toxicity of degradation products. *New J. Chem.* **2019**, *43*, 7294.
(7) Baira, S. M.; Gunupudi, P.; Abbaraju, V.; R, S.; Talluri, M. V. N. K. Study of forced degradation behaviour of cobicistat and atazanavir using LC/ESI/QTOF/MS;a combination of in-sourced and collision-induced dissociation for evaluation of the fragmentation patterns of degradation products. *New J. Chem.* **2018**, *42*, 19113−19128.
(8) *The Japanese Pharmacopoeia XVII*; The Ministry of Health, Labour and Welfare: Japan, 2016.
(9) Kalyankar, G. G.; Desai, P. N.; Prajapati, P. B.; Lodha, S. R.; Joshi, S. V.; Bodiwala, K. B.; Mishra, A. A.; Shah, S. A. Development and validation of stability-indicating RP-HPLC method for estimation of pranlukast hydrate in its laboratory mixture. *J. Chromatogr. Sci.* **2021**, *60*, 179.
(10) Mamata, J.; Devanna, N. Analysis of pranlukast in dosage form by a validated RP HPLC method. *Int. J. Recent Sci. Res.* **2017**, *8*, 22730−22733.
(11) Luan, L.; Sugiyama, T.; Takai, S.; Usami, Y.; Adachi, T.; Katagiri, Y.; Hirano, K. Purification and characterization of pranlukast hydrolase from rat liver microsomes: The hydrolase is identical to carboxylesterase pI 6.2. *Biol. Pharm. Bull.* **1997**, *20*, 71−75.
(12) Brocks, D. R.; Upward, J. W.; Georgiou, P.; Stelman, G.; Doyle, E.; Allen, E.; Wyld, P.; Dennis, M. J. The single and multiple doses of pharmacokinetics of pranlukast in healthy volunteers. *Eur. J. Clin. Pharmacol.* **1996**, *51*, 303−308.
(13) Tang, S.-S.; Ji, M.-j.; Chen, L.; Hu, M.; Long, Y.; Li, Y.-q.; Miao, M.-x.; Li, J.-c.; Li, N.; Ji, H.; Chen, X.-j.; Hong, H. Protective effect of pranlukast on $A\beta_{1-42}$-induced cognitive deficits associated with downregulation of cysteinyl leukotriene receptor 1. *Int. J. Neuropsychiatry* **2014**, *17*, 581−592.
(14) ICH. Stability Testing of New Drug Substances and Products Q1(A) R2. *International Conference on Harmonization*; IFPMA: Geneva, Switzerland, 2003.
(15) ICH. Stability Testing: Photostability Testing of New Drug Substances and Products Q1B. *International Conference on Harmonization*; IFPMA: Geneva, Switzerland, 1996.
(16) ICH. Validation of Analytical Procedures: Text and Methodology Q2 (R1). *International Conference on Harmonization*; IFPMA: Geneva, Switzerland, 2005.
(17) admetSAR2. http://lmmd.ecust.edu.cn/admetsar2/, (accessed 2021).
(18) Luo, Z.; Liu, A.; Liu, Y.; Wang, G.; Chen, X.; Wang, H.; Li, M.; Zhang, H.; Qiu, Y.; Zhai, H. Development of a stability−indicating HPLC method for simultaneous determination of ten related substances in vonoprazan fumarate drug substance. *J. Pharm. Biomed. Anal.* **2018**, *149*, 133−142.
(19) Zhou, D.; Porter, W. R.; Zhang, G. G. Z. Drug Stability and Degradation Studies. In *Theories and Techniques in the Characterization of Drug Substances and Excipients*; Elsevier Inc., 2017; pp 113−149.
(20) Sengupta, P.; Chatterjee, B.; Tekade, R. K. Current regulatory requirements and practical approaches for stability analysis of pharmaceutical products: A comprehensive review. *Int. J. Pharm.* **2018**, *543*, 328−344.
(21) Sengupta, P.; Chatterjee, B.; Tekade, R. K. Current regulatory requirements and practical approaches for stability analysis of pharmaceutical products: A comprehensive review. *Int. J. Pharm.* **2018**, *543*, 328−344.
(22) Vishnuvardhan, C.; Allakonda, L.; Srinivas, R.; Satheeshkumar, N. Forced degradation study of racecadotril: Effect of co-solvent, characterization of degradation products by UHPLC-Q-TOF-MS/MS, NMR and cytotoxicity assay. *J. Pharm. Biomed. Anal.* **2016**, *128*, 9−17.
(23) Singh, D. K.; Sahu, A.; Wani, A. A.; Bharatam, P. V.; Kotimoole, C. N.; Batkulwar, K. B.; Deshpande, A. Y.; Giri, S.; Singh, S. Stability behaviour of antiretroviral drugs and their combinations. 10: LC-HRMS, LC-MS^n, LC-NMR and NMR characterization of fosamprenavir degradation products and in silico determination of their ADMET properties. *Eur. J. Pharm. Biopharm.* **2019**, *142*, 165−178.
(24) Baira, S. M.; Gunupudi, P.; Abbaraju, V.; R, S.; Talluri, M. V. N. K. Study of forced degradation behaviour of cobicistat and atazanavir using LC-ESI-QTOF-MS; a combination of in-sourced and collision-induced dissociation for evaluation of the fragmentation patterns of degradation products. *New J. Chem.* **2018**, *42*, 19113−19128.
(25) International Standard ISO. *Biological Evaluation of Medical Devices—Part 5: Tests for In Vitro Cytotoxicity*, 2009; pp 10993−10995.
(26) Kahnt, A. S.; Rörsch, F.; Diehl, O.; Hofmann, B.; Lehmann, C.; Steinbrink, S. D.; Angioni, C.; Geisslinger, G.; Grösch, S.; Steinhilber, D.; Maier, T. J. Cysteinyl leukotriene-receptor-1 antagonists interfere with PGE_2 synthesis by inhibiting mPGES-1 activity. *J. Biochem. Pharmacol. Res.* **2013**, *86*, 286−296.
(27) Wang, J.; Wang, C.; Li, X.; Kong, L.; Gao, K.; Liu, R.-Y. The effects of anti-asthma drugs on the phagocytic clearance of apoptotic eosinophils by A549 cells. *Respir. Med.* **2009**, *103*, 1693−1699.
(28) Verstraelen, S.; Bloemen, K.; Nelissen, I.; Witters, H.; Schoeters, G.; Heuvel, R. V. D. Cell types involved in allergic asthma and their use in in vitro models to assess respiratory sensitization. *Toxicol. in Vitro* **2008**, *22*, 1419−1431.
(29) Fang, S.-h.; Lin, K.-n.; Huang, X.-q.; Lu, Y.-b.; Zhang, W.-p.; Wei, E.-q. Nuclear translocation of cysteinyl leukotriene receptor 1 is involved in oxygen-glucose deprivation-induced damage to endothelial cells. *Acta Pharmacol. Sin.* **2012**, *33*, 1511−1517.
(30) Sambale, F.; Lavrentieva, A.; Stahl, F.; Blume, C.; Stiesch, M.; Kasper, C.; Bahnemann, D.; Scheper, T. Three dimensional spheroid cell culture for nanoparticle safety testing. *J. Biotechnol.* **2015**, *205*, 120−129.
(31) Kesharwani, P.; Gajbhiye, V.; K Tekade, R.; K Jain, N. Evaluation of dendrimer safety and efficacy through cell line studies. *Curr. Drug Targets* **2011**, *12*, 1478−1497.
(32) Yousefian Rad, E.; Homayouni Tabrizi, M.; Ardalan, P.; Seyedi, S. M. R.; Yadamani, S.; Zamani-Esmati, P.; Haghani Sereshkeh, N. Citrus Lemon essential oil nanoemulsion (CLEONE), a safe cell-depended apoptosis inducer in human A549 lung cancer cells with anti-angiogenicactivity. *J. Microencapsul.* **2020**, *37*, 394−402.
(33) Gorycki, P. D.; Annan, B. W.; Kuo, G. Y. Substitutes Benzopyrans. U.S. Patent 5939447 A, 1999.
(34) Prajapati, K. J.; Kothari, C. Development and validation of a stability indicating LC-MS/MS method for the determination of clenbuterol HCl. *Drug Res.* **2020**, *70*, 552−562.
(35) Prajapati, K. J.; Kothari, C. S. First report on clorprenaline HCl degradation products: Identification and characterization by LC-MS/MS. *J. Iran. Chem. Soc.* **2020**, *17*, 1027−1039.
(36) Chavan, B. B.; Sawant, V.; Borkar, R. M.; Ragampeta, S.; Talluri, M. V. N. K. Isolation and structural characterization of degradation products of afatinib dimaleate by LC-Q-TOF/MS/MS and NMR: cytotoxicity evaluation of afatinib and isolated degradation products. *J. Pharm. Biomed. Anal.* **2019**, *166*, 139−146.
(37) Zhang, M.; Liu, Y.; Chen, J.; Liu, H.; Lu, X.; Wu, J.; Zhang, Y.; Lin, Y.; Liu, Q.; Wang, H.; Guo, L.; Gao, R.; Xu, B.; Xie, J. Sensitive untargeted screening of nerve agents and their degradation products using liquid chromatography-high resolution mass spectrometry. *Anal. Chem.* **2020**, *92*, 10578.
(38) Lei, Y.; Jin, B.; Ma, C.; Zhang, T.; Li, T. Identification of forced degradation products of tedizolid phosphate by liquid chromatography/electrospray ionization tandem mass spectrometry. *J. Pharm. Biomed. Anal.* **2017**, *139*, 221−231.

https://doi.org/10.1021/acs.chemrestox.1c00222
Chem. Res. Toxicol. 2022, 35, 1206−1219

(39) Mehta, S.; Shah, R. P.; Priyadarshi, R.; Singh, S. LC and LC-MS/TOF studies on stress degradation behaviour of candesartan cilexetil. *J. Pharm. Biomed. Anal.* **2010**, *52*, 345−354.
(40) Mehta, S.; Shah, R. P.; Singh, S. Strategy for identification and characterization of small quantities of drug degradation products using LC and LC-MS: Application to valsartan, a model drug. *Drug Test. Anal.* **2010**, *2*, 82−90.
(41) Li, M. *Organic Chemistry of Drug Degradation*; Royal Society of Chemistry: Ringoes, New Jersey, 2012; pp 16−197.

https://doi.org/10.1021/acs.chemrestox.1c00222
Chem. Res. Toxicol. 2022, 35, 1206−1219